

# Characterization of Hydrogen DRI Samples From ZESTY Process



## Authors

**Bintang A. Nuraeni** (top left), Research Fellow, Swinburne University of Technology, Melbourne, Vic., Australia  
bnuraeni@swin.edu.au

**Isis R. Ignacio** (top right), CSIRO Early Research Career Postdoctoral Fellow, CSIRO Mineral Resources, Brisbane, Qld., Australia  
isis.rosagnacio@csiro.au

**Geoffrey A. Brooks** (middle left), Professor of Engineering, Department of Mechanical and Product Design Engineering, Swinburne University of Technology, Melbourne, Vic., Australia  
gbrooks@swin.edu.au

**Deddy C. Nababan** (middle right), Postdoctoral Fellow, CSIRO Mineral Resources, Vic., Australia  
deddy.nababan@csiro.au

**M.A. Rhamdhani** (bottom left), Professor, Department of Mechanical and Product Design Engineering, Swinburne University of Technology, Melbourne, Vic., Australia

**Matt E. Boot-Handford** (bottom right), Chief Scientist, Calix Ltd., Pymble, NSW, Australia  
mboot-handford@calix.global

**Y. Xia**, Calix Ltd., Pymble, NSW, Australia

**T. Dufty**, Calix Ltd., Pymble, NSW, Australia

**M.G. Sceats**, Calix Ltd., Pymble, NSW, Australia

The ZESTY Ironmaking process involves the use of Calix's flash calcination technology to reduce iron ore fines to iron in a hydrogen atmosphere between 600 and 1,050°C. In 2022, Calix ran a series of proof-of-concept campaigns at its pilot plant facility using a range of iron ores, particle sizes, process temperatures, hydrogen flowrates at throughputs up to 100 kg/hour in semi-continuous mode. Detailed x-ray diffraction, scanning electron microscopy-energy-dispersive x-ray spectroscopy, optical microscopy and chemical analysis of the samples revealed key aspects of the process, showing that hematite-goethite ores could be readily metallized in the process. A modified thermogravimetric technique was able to duplicate closely the kinetic behavior observed in plant trials.

## Introduction

Steelmaking is one of the world's largest industrial sectors, being responsible for 1.88 billion metric tons of crude steel production in 2022, and one of the most polluting sectors (after the cement industry), generating 7–9% of the total carbon monoxide (CO<sub>2</sub>) emissions.<sup>1</sup> The main method to produce primary iron is via blast furnace (more than 90% of the operations);<sup>2</sup> however, due to the environmental impact caused by its operation, new methods are being developed. Using hydrogen as a reduction agent, possibly produced from renewable energy, is a future alternative to fossil fuels, and it has been widely investigated. The use of hydrogen in iron ore reduction reactions has been studied for many decades and industries have implemented procedures combining different techniques and reactors (rotary furnace, plasma, fixed and fluidized beds), for example.<sup>3</sup>

A new ironmaking technology was developed in which fine iron ore concentrate is suspended and directly reduced under gaseous atmosphere in a flash reactor.<sup>4,5</sup> The advantage of this flash ironmaking process is to produce direct reduced iron (DRI) at a high metallization degree within few seconds of residence time,<sup>4</sup> under

lower temperatures than in the blast furnace (as low as 800°C<sup>6</sup>) and avoiding the agglomeration (sintering and pelletizing) steps. However, from the thermodynamic point of view, using hydrogen as a reductant can lead to changes in the stability of iron formation reaction, requiring higher temperatures.<sup>7</sup> Furthermore, most of the knowledge on gas-solid reaction of iron ores comes from larger samples, and the behavior and diffusion mechanisms of small particles (–150 μm) under a hydrogen atmosphere is unclear.

This work aims to provide detailed analysis of the kinetics and micro-mechanism of the reactions of several Australian ores, including appropriate metallurgical characterization. For that, a series of laboratory-scale tests was conducted to evaluate a few iron ores for their feasibility to be reduced by hydrogen and to identify the optimum process conditions that can inform a pilot plant testing. Reduction experiments were carried out by suspending microparticles of different ores, in a varied size range, in a thermogravimetric analyzer (TGA) furnace in a diluted hydrogen atmosphere. The weight loss of the samples after reaction was measured and the effects of temperature, hold time and

flowrate was observed. Different cooling methods were also investigated.

## ZESTY Iron Process

The Zero Emission Steel TechnologY (ZESTY) is a novel  $H_2$ -direct reduction method for producing iron that relies on the exclusive Calix Flash Calcination (CFC) technology. In this method,  $H_2$  is introduced in a counterflow configuration at the base of the reactor and fine iron ore (usually below 500  $\mu m$ ) is fed at the top. As the iron ore powder passes through the reactor, it is flash heated and reduced to a DRI product. The DRI can then be briquetted into hot briquetted iron (HBI) for export to steelmakers, or it can be treated in a melting plant to separate gangue from iron. The introduction of  $H_2$  in a counterflow configuration guarantees the establishment of a concentration gradient within the process, with the highest concentration of  $H_2$  at the reactor's base. This ensures the effective use of  $H_2$ , promoting high conversions to metallic iron and increased productivity per reactor tube or module. A cyclone and dedusting system remove fines embedded in the exhaust gases, which are then reinjected into the process.<sup>8</sup>

The ZESTY process has many advantages when compared to other DRI processes. A high degree of metallization can be achieved over noticeably shorter residence times (often 60 seconds) and lower-temperature operation than a conventional blast furnace, for example. ZESTY's ability to facilitate fast reaction kinetics of iron ore fines eliminates the need for agglomeration or pelletization. Reduced processing temperatures and shorter residence periods also reduces the operational problems caused by sticking, which can impair solid flow in shaft furnace operations and cause defluidization in fluidized bed DRI methods.<sup>8</sup> Additionally, because of ZESTY's innovative indirect heating method, effective electrification is made possible while also allowing hydrogen to be easily recovered and used only as a reductant rather than as fuel. This potentially allows for the most cost-effective and efficient use of hydrogen by lowering operating temperatures.<sup>9</sup> Calix is developing its ZESTY process to utilize a recirculation loop to feed unreacted  $H_2$  back into the process to meet the theoretical minimum hydrogen use of 54 kg/ton hydrogen direct reduced iron (H-DRI) for a hematite ore.<sup>9</sup> The program is now in pilot test phase, with preliminary findings being obtained at Calix's Centre for Technology Development located in Victoria, Australia. Fig. 1 shows a schematic of the ZESTY ironmaking process. An earlier publication by the authors outlines results from pilot plant studies and

indicates that metallization above 90% can be achieved in the reactor for goethite/hematite ores.<sup>9</sup>

## Experimental

### Iron Ores for Metallization Degree Determination

A number of DRI samples produced during the first Calix trial were handled for analysis at Swinburne University. The samples originated from three different iron ores (siderite, goethite/hematite, magnetite) and reduced under different temperature and  $H_2$  concentrations. Table 1 shows the complete list of sample identifications and reduction conditions. These iron ores were characterized in this study using different metallization degree determination techniques. DRI 1, 2 and 3 were derived from the same parent ore, a siderite. The difference among them is the conditions in which they were processed in the ZESTY pilot plant. DRI 4 comes from hematite/goethite ore and DRI 5 comes from magnetite ore. [A], [B] and [C] refer to the duplicate or triplicate samples.

### Iron Ores for Kinetic Experiment

Three types of ore (Blends 1–3) were used in this study to examine the effect of iron ore and particle size to the reduction kinetics, shown in Table 2. The samples were identified by Blend + a number + a letter, where the number corresponds to the ore used and the letter to the particle size range analyzed. Thus, sample Blend 2C, for example, were produced using goethite within the 63–100  $\mu m$  particle size range.

Figure 1

### ZESTY ironmaking process.<sup>8</sup>

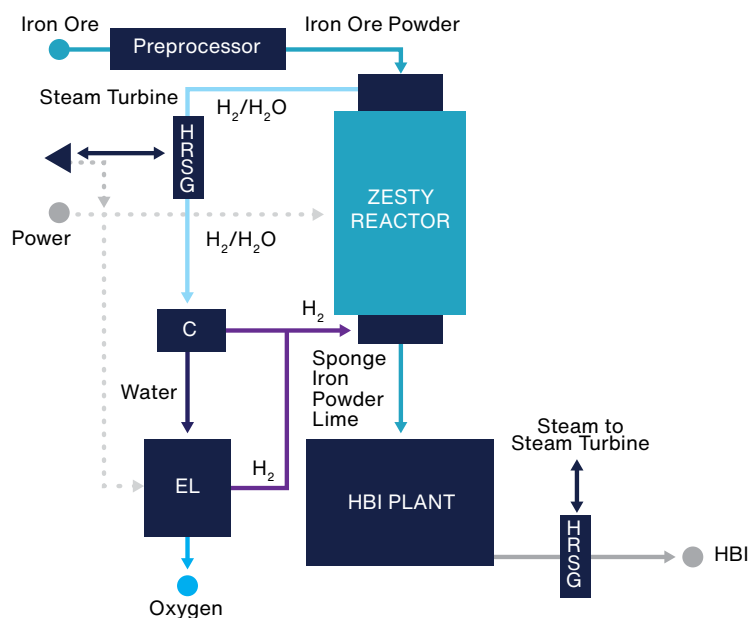


Table 1

List of Direct Reduced Iron (DRI) Samples Used for Metallization Degree Determination

| Sample ID                   | Processing temperature (°C) | Target H <sub>2</sub> /reducible O ratio |
|-----------------------------|-----------------------------|--|
| DRI 1_Siderite [A]          | 950                         | 2/1                                      |
| DRI 1_Siderite [B]          |                             |  |
| DRI 2_Siderite [A]          |                             |  |
| DRI 2_Siderite [B]          | 950                         | 2/1                                      |
| DRI 2_Siderite [C]          |                             |  |
| DRI 3_Siderite [A]          |                             |  |
| DRI 3_Siderite [B]          | 750                         | 2/1                                      |
| DRI 4_Hematite/Goethite_[A] |                             |  |
| DRI 4_Hematite/Goethite_[B] |                             |  |
| DRI 5_Magnetite_[A]         | 1,050                       | 2/1                                      |
| DRI 5_Magnetite_[B]         |                             |  |

Table 2

Iron Ores Used for Kinetic Experiment, With the Particle Size Range

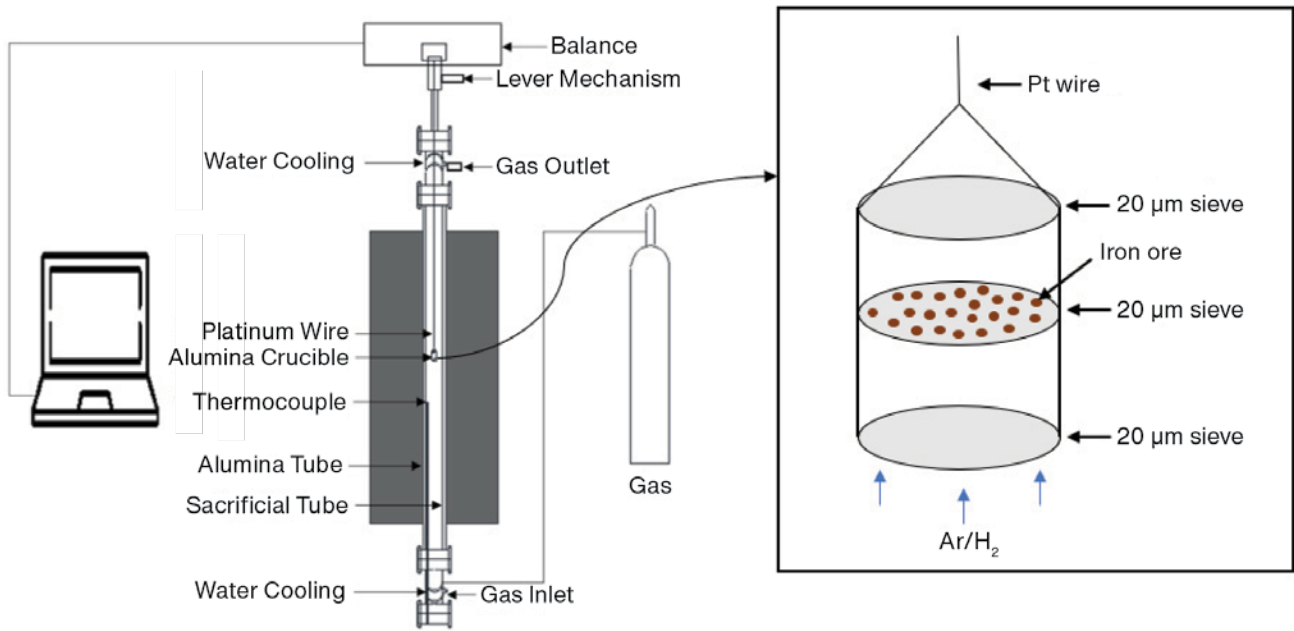
| Sample ID | Ore type          | Size (µm) |        |     |
|-----------|-------------------|-----------|--------|-----|
|           |                   | A         | B      | C   |
|           |                   | 125–300   | 63–100 | <38 |
| Blend 1   | Goethite/Hematite | x         | x      | x   |
| Blend 2   | Goethite          | x         | x      | x   |
| Blend 3   | Magnetite         | x         | x      | x   |

Kinetic Experiment Setup

DRI product was made on a laboratory scale aiming to simulate the ZESTY process. A TGA furnace was used in this experiment, which consisted of a vertical tube furnace with a control system, and a precision balance (FX-300i with 1 mg accuracy) at the top of the furnace to measure the weight loss of the sample during the reaction. The same setup was previously used by Ignacio (2022)<sup>10</sup> and Nuraeni (2022)<sup>11</sup> for reducibility and kinetic studies. Fig. 2 shows the layout of the TGA apparatus.

Figure 2

Layout of thermogravimetric analyzer (TGA) apparatus and sample holder.<sup>11</sup>



The iron ore sample in powder form, weighing 0.100 g ( $\pm 0.05$  g), was placed inside an alumina crucible with a stainless steel screen between to hold the sample, and another two to avoid the escaping of samples from the top and bottom (Fig. 3a). The screens allowed the gas to flow more easily through the particles, simulating the plant tests. The powder was spread carefully and evenly in a thin layer onto the screen to avoid agglomeration after heating. The crucible was held by a platinum wire basket suspended from the top water-cooled flange and placed in the hot zone of the furnace. The furnace was sealed, and argon gas was purged to maintain a neutral atmosphere before and after each run. After a few minutes, the

reducing atmosphere was created by injecting a mixture of  $H_2/N_2$  (15% and 85%, respectively). All the tests were conducted at 950°C for 5–30 minutes. The weight loss was recorded continuously every 0.125 second using WinCT software (A&D, Japan) for a varied time.

### Characterization Techniques

**Optical Microscopy (OM):** OM was used in this study to allow direct observation of the material's cross-section, providing insights on the mineral phases and pore size and shape. The samples were prepared by embedding the sample in resin, followed by plane grinding and polishing

Table 3

#### Metallization Degree Techniques for Determination of Metallic Iron

| Characteristic                | Method  |   |  |   |  |  |   |
|-------------------------------|---|---|--|---|--|--|---|
|                               | ISO 16878: 2016   | ISO 5416:2006   | XRF  | XRD   | ICP-AES  | ISO 2597-1:2006  | ASTM E246-10 (2015)   |
| Metallic Fe                   | ✓   | ✓   | ✓  | ✓   | ✓  | —  | —   |
| Total Fe                      | —   | —   | ✓  | —   | ✓  | ✓  | ✓   |
| Description                   | Iron (III) chloride titrimetric method  | Bromine-methanol titrimetric method   | Determination of elemental composition of materials by XRF   | Determination of crystallographic structure of a material by x-ray radiation  | Emission spectroscopy technique using a plasma   | Titrimetric method after tin (II) chloride reduction   | Dichromate titration  |
| Applicable range (Fe content) | 57.5–90.5%  | 15–95%  | Unlimited  | Unlimited   | Unlimited  | 30–72%   | 30–95%  |
| Advantages                    | <ul style="list-style-type: none"> <li>High precision</li> </ul>  | <ul style="list-style-type: none"> <li>High precision applicable for wide range of Fe content</li> </ul>                                      | <ul style="list-style-type: none"> <li>Rapid process</li> <li>Generally nondestructive</li> <li>Simple and fast sample preparation, low running costs</li> </ul> | <ul style="list-style-type: none"> <li>Rapid process</li> <li>Simple sample preparation</li> <li>Straight-forward interpretation</li> </ul> | <ul style="list-style-type: none"> <li>Fast and simultaneous determination of multielement</li> <li>Low running costs</li> </ul> | <ul style="list-style-type: none"> <li>High precision low toxicity chemicals</li> </ul>  | <ul style="list-style-type: none"> <li>High precision applicable for wide range of Fe content</li> </ul>  |
| Dis-advantage                 | <ul style="list-style-type: none"> <li>Limited applicability of Fe content range</li> <li>Waste products</li> </ul> | <ul style="list-style-type: none"> <li>Hazards associated with bromine methanol</li> <li>Waste products</li> <li>High running cost</li> </ul> | <ul style="list-style-type: none"> <li>Not recommended, semi-quantitative</li> </ul>   | <ul style="list-style-type: none"> <li>Not recommended, semi-quantitative</li> </ul>  | <ul style="list-style-type: none"> <li>High continuum emission background; this constrains detection precision</li> </ul>        | <ul style="list-style-type: none"> <li>Hazards associated with use of strong acids, mercury</li> <li>Involving high temperature (800°C of sample decomposition)</li> <li>Waste byproducts</li> </ul> | <ul style="list-style-type: none"> <li>Hazards associated with use of strong acids, and highly toxic <math>H_2S</math></li> <li>Involving high temperature (900°C of sample decomposition)</li> <li>Waste byproducts</li> </ul> |

\* Determination of metallic iron by XRF and XRD should only be considered as semi-quantitative.

\*\* By cupric chloride digestion, solid metallic Fe replaces the  $Cu^{2+}$  in the solution and becomes  $Fe^{2+}$ . Solid metallic Fe content is determined by elemental quantification of the Fe content in the solution.

using an automated polisher. The polished samples were placed on a moving stepping stage attached to an optical microscope (Olympus BX61) embedded with OLYMPUS Stream Version 510 software.

**Scanning Electron Microscopy (SEM):** For SEM analysis, the samples in powder form were attached to a carbon tape to prevent electrostatic charging and ensure uniform emission of secondary electrons. Backscattered electron (BSE) photomicrographs were taken at different magnifications, conducted under high vacuum conditions, with a working distance of 10 mm, a high voltage of 15 kV, an emission current of 158  $\mu$ A, a pressure of  $1.1 \times 10^{-6}$  Torr, and a gun pressure of  $9.1 \times 10^{-10}$  Torr.

**X-Ray Diffraction (XRD):** For the analysis of x-ray powder diffraction, the samples were ground in a mortar and pestle to create a uniform powder. Subsequent analyses were performed using a Bruker XRD (Bruker AXS GmbH) instrument, employing Cu K  $\alpha$  radiation at 40 kV and 40 mA. The scanning range spanned  $2\theta$  angles from 15 to  $140^\circ$ , with a scanning step of  $0.02^\circ$  and a dwell time of 1 second. Identification of XRD peaks for individual phases was achieved through indexing and matching the diffraction patterns with known spectra from the International Centre for Diffraction Data Powder Diffraction File.

### Metallization Degree Determination Techniques

The metallization degree is a measure of the extent to which iron ore has been reduced to metallic iron during the ironmaking process. It is an important parameter in assessing the efficiency of the reduction process and the quality of the final iron product. Several tests are commonly used to determine the reduction degree and the metallization degree of iron ores. TGA, for example, measures the weight loss of a sample as it is heated. The reduction of iron ore can be monitored by observing the weight loss associated with the release of oxygen during the reduction process. Determination of metallic iron involves quantifying the amount of metallic iron present in the iron ore sample, usually by chemical methods. The choice of test method may depend on factors such as the specific ironmaking process, the nature of the iron ore and the required level of precision. Additionally, these tests are often conducted in combination to obtain a comprehensive understanding of the metallization degree of iron ores. Table 3 summarizes the common techniques, providing a brief description, applicable range of Fe content, advantages and drawbacks of each technique used to determine metallic iron and total iron, respectively.

In this work, five different DRI samples, from different parent ores were analyzed by four techniques:

1. Method 1: Cupric chloride digestion method by inductively coupled plasma atomic emission spectroscopy (ICP-AES). Samples were prepared using a peroxide fusion technique or cupric chloride digestion method for determination of the

total iron and metallic iron contents respectively.<sup>9,12</sup> This test was conducted by Spectrometer Services Pty Ltd. in Melbourne.

2. Method 2: Bromine-methanol extraction and determination of metallic iron by ICP-AES.

For each sample, 500 mg was mixed with 5 ml of bromine and 95 ml of anhydrous methanol. Samples were mixed for one hour in sealed Erlenmeyer flasks using a Ratek platform mixer. The post extraction solids were filtered using a 47-mm-diameter 0.45  $\mu$ m Millipore Durapore membrane and Millipore vacuum filtration apparatus. The bromine methanol filtrate was quantitatively transferred to a 400 ml beaker and allowed to evaporate to dryness with heat. The residue was digested in nitric acid with heat and Milli-Q water. The clear solutions were made to a 100 ml volume in 5% nitric acid and Milli-Q water. These solutions were diluted tenfold and analyzed for iron using the Agilent 5900 ICP-AES. The test was conducted by the CSIRO Clayton in Melbourne.

3. Method 3: Bromine-methanol titrimetric determination of metallic iron using ISO Standard 5416:2006.<sup>13</sup> The test was conducted by the CSIRO Clayton in Melbourne.
4. Method 4: Total iron content by XRF (including loss on ignition).

For each sample, 0.36 g was fused with lithium borate flux. The fused beads were analyzed using the Bruker S8 Tiger XRF instrument. The loss on ignition was performed on 1.1 g of material heated to  $1,025^\circ\text{C}$  overnight in air, in a muffle furnace. The test was conducted by CSIRO Clayton in Melbourne.

## Results and Discussion

### Metallization Degree Investigation

The metallization degree represents the overall conversion of iron ore into metallic iron, considering both the reduction of iron oxide and subsequent melting of the metallic iron. It recognizes the percentage of iron ore that has been transformed into metallic iron, regardless of whether the iron oxide has been completely reduced. In this work, the metallization degree was calculated by Eq. 1. Table 4 shows the metallic Fe (%) and total Fe (%) results obtained from methods 1 to 4. Fig. 5 shows the metallization degree (%) for the DRI samples. Boot-Handford et al. (2023) discussed in their previous publication the effects of temperature on the metallization degree of the DRI samples.<sup>9</sup> Here, the hematite/goethite DRI samples presented the highest metallization degree, while magnetite DRI samples showed the lowest, as expected. Although both samples were processed under same conditions, the mineralogical nature of the ores are different. Hematite/goethite ores presents high porosity,



Table 4

## Metallic Fe (%) and Total Fe (%) Results

| Sample ID                       | Method 1<br>(ICP-AES, Cupric Chloride) |              | Method 2<br>(ICP-AES,<br>Bromine-Methanol) | Method 3<br>(ISO 5416) | Method 4<br>(XRF) |
|---------------------------------|--|--------------|--|------------------------|-------------------|
|                                 | Metallic Fe (%)                        | Total Fe (%) | Metallic Fe (%)                            | Metallic Fe (%)        | Total Fe (%)      |
| DRI 1_Siderite [A]              | 74.5                                   | 76.5         | 68.6                                       | --                     | 78.5              |
| DRI 1_Siderite [B]              | 72.8                                   | 77.5         | 68.8                                       | --                     | 77.8              |
| DRI 2_Siderite [A]              | 63.9                                   | 71.0         | 57.3                                       | 57.6                   | 76.1              |
| DRI 2_Siderite [B]              | 66.0                                   | 75.2         | 57.5                                       | 57.9                   | 75.5              |
| DRI 2_Siderite [C]              | 65.8                                   | 76.0         | 55.9                                       | 56.6                   | --                |
| DRI 3_Siderite [A]              | 45.5                                   | 72.7         | 34.7                                       | --                     | 71.9              |
| DRI 3_Siderite [B]              | 46.9                                   | 73.8         | 36.3                                       | --                     | 71.5              |
| DRI 4_Hematite/<br>Goethite [A] | 69.1                                   | 79.4         | 65.1                                       | 66                     | 79.7              |
| DRI 4_Hematite/<br>Goethite [B] | 71.0                                   | 81.1         | 65.2                                       | 66.5                   | 78.0              |
| DRI 5_Magnetite [A]             | 48.7                                   | 80.9         | 43.7                                       | 43.3                   | 81.5              |
| DRI 5_Magnetite [B]             | 49.9                                   | 79.7         | 43.5                                       | 43.8                   | 82.9              |

\*[A], [B] and [C] refers to the duplicate or triplicate samples

increasing the surface area facilitating the reaction to happen, while magnetite ores are dense and less reducible. The siderite DRI presented more diverse metallization degrees, reaching numbers as high as hematite/goethite samples and low as magnetite samples. Higher processing temperature (for DRI 1) enhanced the reduction rates and improved the kinetics, when compared to the lower temperatures (for DRI 3).

The results from method 2 (ICP-AES, Bromine-Methanol) and 3 (ISO 5416) were comparable, while the method 1 (ICP-AES, Cupric Chloride) presented higher values. This indicates that ICP-AES can be used to investigate the metallization degree of DRI samples with excellent accuracy level. It is worth noting that the lower metallic iron from the bromine methanol method might be because of slow reoxidation but this needs further investigation.

$$\text{Metallization degree (\%)} = \frac{\text{Metallic Fe}}{\text{Total Fe}} \times 100$$

(Eq. 1)

Figure 3

Averaged metallization degree of different type of ore by different methods (%).

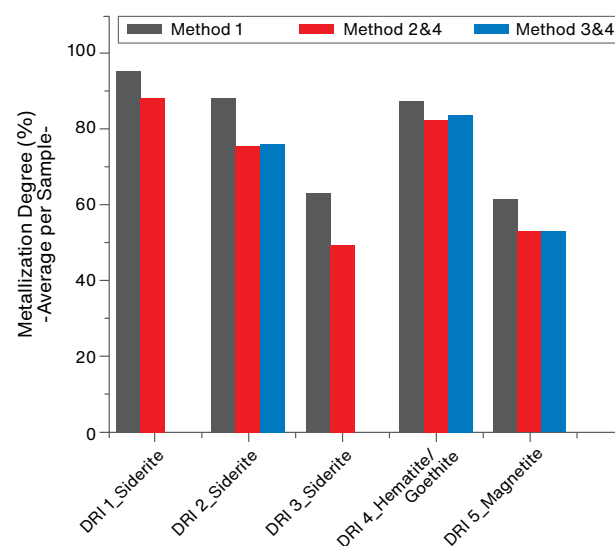
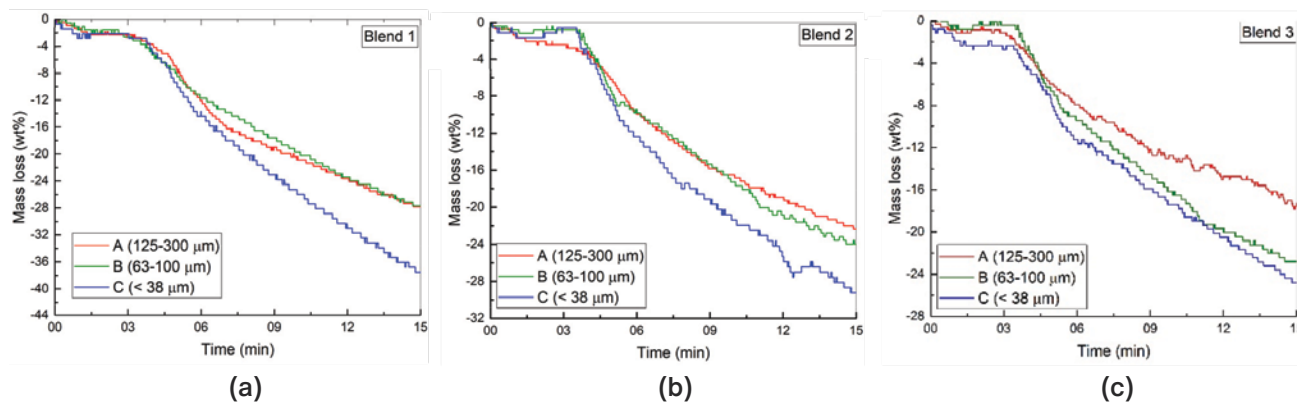


Figure 4

Mass loss during reduction reaction by particle size of Blend 1, (a) Blend 2 (b) and Blend 3 (c).



### Effect of Particle Size and Iron Ore on Reduction Kinetics

The mass loss curves of different particle sizes of Blends 1, 2 and 3 are shown in Fig. 4a, 4b and 4c, respectively. Across all type of ore, similar profiles were observed during the first 3 to 4 minutes, indicating that the mass loss of these three ores changed slowly during the initial period due to moisture release and no significant reduction reaction occurred. Overall, finer particle size favored higher mass loss, which is most likely due to better gas-solid contact between the ore and  $\text{H}_2$ . Blend 1 and Blend 2 behaved similarly, where the finest particles show significantly higher mass loss, while middle and coarse particles show nearly identical mass loss. The similarity of the two ores was likely due to the morphology of the raw ore (Figs. 5 and 6) which exhibit porous characteristics. Blend 3 behaved differently from Blends 1 and 2, where the coarse particles show significantly lower mass loss, while finest and middle size particle show similar mass loss. Blend 3 raw ore has denser morphology (Fig. 7) compared to Blends 1 and 2.

The lower reduction degree of the magnetite samples was also observed from DRI samples produced during the ZESTY pilot testing campaign. This phenomenon can be attributed to the denser and

Figure 5

Cross-section SEM images of Blend 1 (raw compared to reduced samples in different particle sizes, A: 125–300  $\mu\text{m}$ , B: 63–100  $\mu\text{m}$ , C: <38  $\mu\text{m}$ ), light/white-color phase: metallic Fe, gray-color phase: iron oxide.

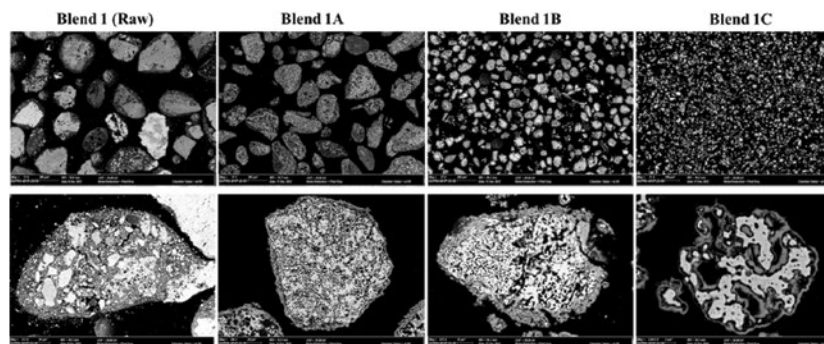


Figure 6

Cross-section SEM images of Blend 2 (raw compared to reduced samples in different particle sizes, A: 125–300  $\mu\text{m}$ , B: 63–100  $\mu\text{m}$ , C: <38  $\mu\text{m}$ ), light/white-color phase: metallic Fe, gray-color phase: iron oxide.

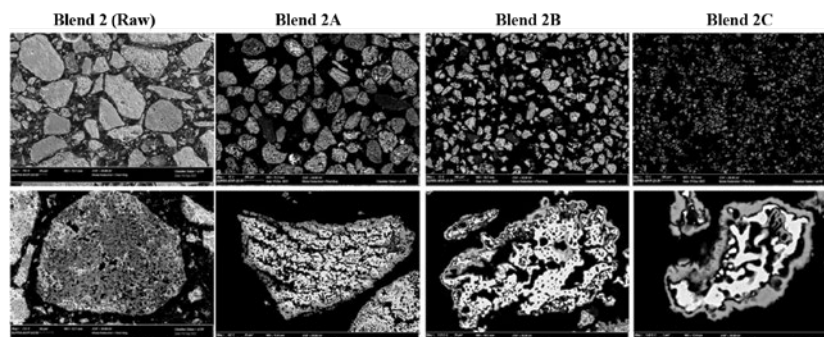
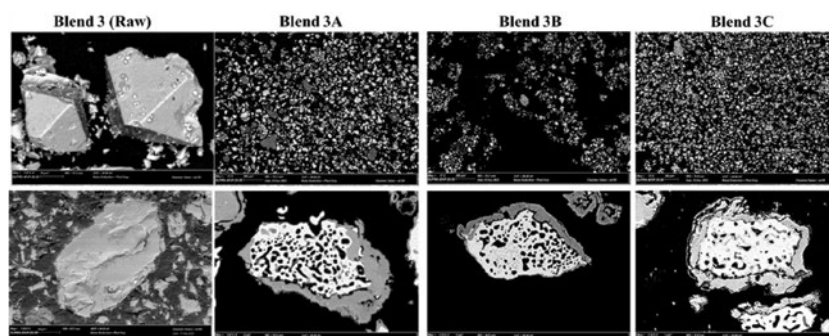


Figure 7

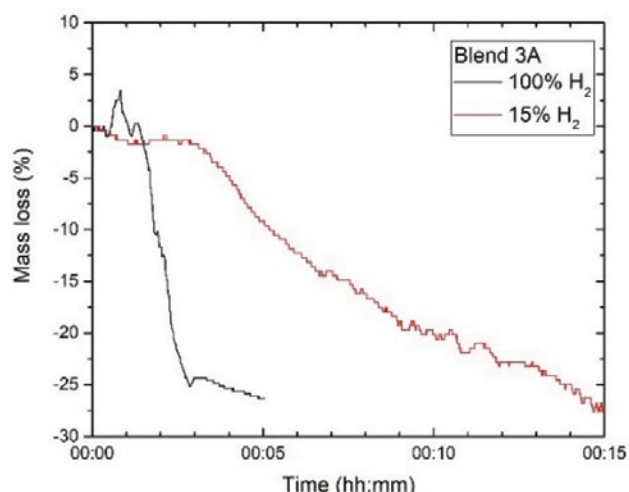
Cross-section SEM images of Blend 3 (raw compared to reduced samples in different particle sizes, A: 125–300  $\mu\text{m}$ , B: 63–100  $\mu\text{m}$ , C: <38  $\mu\text{m}$ ), light/white-color phase: metallic Fe, gray-color phase: iron oxide.



less porous nature of the magnetite sample, leading to a smaller reaction interface and a longer mean path length for solid-state diffusion compared to other ore samples. In contrast, goethite/hematite ores contain “calcinable” phases that can be calcined, releasing gaseous species upon heating. This process creates internal porosity and increases the surface area available for reactions, thereby promoting faster reaction kinetics compared to the denser and less porous magnetite ore.<sup>9</sup> Particle size significantly influenced the reduction degree of all three types of ore. Nonetheless, the benefit of smaller particle size (< 38  $\mu\text{m}$ ) was more prominent in increasing the reduction degree of the more porous ores (Blends 1 and 2). On the other hand, for the denser ore (Blend 3), larger particle size (125–300  $\mu\text{m}$ ) notably hindered reduction. However, only

Figure 8

Mass loss of Blend 3A/magnetite (125–300  $\mu\text{m}$ ) reduction by 100%  $\text{H}_2$ , 950°C, 5 minutes.



with slightly smaller particle size (<100  $\mu\text{m}$ ), the reduction degree of magnetite could be significantly increased.

### Effect of $\text{H}_2$ Partial Pressure

Fig. 8 and Table 4 show the mass loss comparison of magnetite reduction at 950°C by different partial pressure of 15%  $\text{H}_2$  and 100%  $\text{H}_2$ . The reduction by 100%  $\text{H}_2$  resulted in a similar mass loss within 5 minutes, indicating a faster rate (3 times) compared to 15%  $\text{H}_2$  within 15 minutes. While the 15%  $\text{H}_2$  reduction underwent a slow mass loss during the first 3–4 minutes, this slow period occurred only in the first minute by 100%  $\text{H}_2$ . The significant mass loss at 100%  $\text{H}_2$  happened between 2 to 3 minutes, continued by a slower rate after minute 3. The rate change at minute 3 could be due to the change of reduction mechanism. During the first 2 minutes, reduction occurred faster due to a sufficient exposure of iron oxide/gas interface. After a substantial iron layer was formed, the reduction slowed down due to the formation of a dense iron layer, which inhibited further iron oxide/gas reaction. Unlike the curve shift observed at 100%  $\text{H}_2$ , the mass loss at 15%  $\text{H}_2$  showed a gradual rate after the first 3–4 minutes. This may indicate that the overall mechanism after minute 4 was governed by a single mechanism. Figs. 9a and 9b show the cross-section images of magnetite samples reduced by 15%  $\text{H}_2$  and 100%  $\text{H}_2$ , respectively.

Previous studies<sup>14–16</sup> have also observed a similar phenomenon, wherein the reduction rate notably decreased when solid-state diffusion of oxygen (SSDO) governed the reduction of iron oxide. For instance, a study by Kim (2013)<sup>16</sup> found that the  $\text{H}_2$  reduction of magnetite at 1,000°C slowed down after 2.5 minutes. Initially, the reduction was controlled by interfacial chemical reaction (ICR) (<2.5 minutes), but it transitioned to mixed control

Table 4

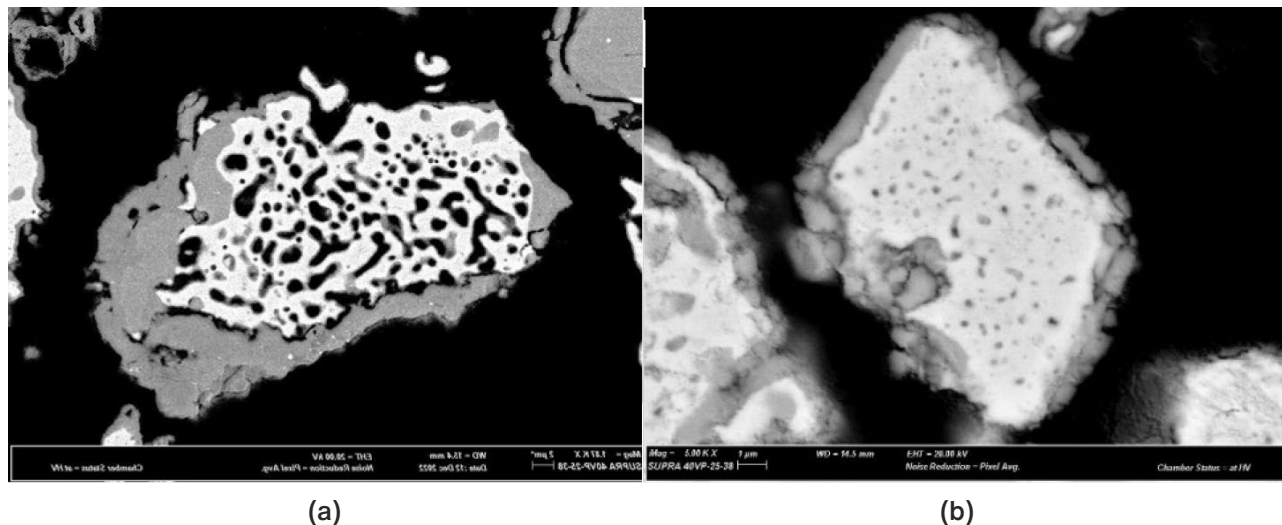
Mass Change of Blend 3A/Magnetite (125–300  $\mu\text{m}$ ) Reduction by 100%  $\text{H}_2$ , 950 °C

| Sample ID | Ore type  | Particle size ( $\mu\text{m}$ ) | $\text{H}_2$ partial pressure | Time (min) | Mass chg (%) |
|-----------|-----------|---------------------------------|-------------------------------|------------|--------------|
| Blend 3E  | Magnetite | <38                             | 15%                           | 15         | -26          |
| Blend 3E  | Magnetite | <38                             | 100%                          | 5          | -25          |



Figure 9

SEM images of Blend 3 magnetite reduction at 950°C by 15% H<sub>2</sub>, 15 minutes (a) and 100% H<sub>2</sub>, 5 minutes (b), light/white-color phase: metallic Fe, gray-color phase: iron oxide.



(ICR and gaseous mass transport (GMT)) as a significant product layer formed and the resistance to GMT became significant. In summary, the slower reduction rate may stem from both the low driving force of diffusion due to the low oxygen solubility in iron at equilibrium and the low oxygen diffusivity through the iron layer.

## Conclusions

The following conclusions were drawn from the study:

1. Determining the degree of metallization can vary depending on factors such as the ironmaking process, the characteristics of the iron ore and the desired level of accuracy. Results obtained through method 2 (ICP-AES with Bromine-Methanol) and method 3 (ISO 5416) were found to be comparable, whereas method 1 (ICP-AES with Cupric Chloride) yielded higher values. This suggests that ICP-AES is a reliable technique for assessing the metallization degree of DRI samples with a good degree of precision.
2. Reduction of three types of iron ores by H<sub>2</sub> has been carried out at 950°C. Raw ore morphology significantly affected the degree of reduction where porosity determined the reduction mechanism. Blend 1 and Blend 2 have a more porous structure compared to Blend 3, which contributed to faster kinetics (mass loss) and a higher degree of reduction. Particle size also played an important role in the reduction degree of all three types of ore. However, the advantage of small particle size (<38 μm) was more pronounced to the reduction degree of more porous ores (Blends 1 and 2). For the denser ore (Blend 3), larger particle size (125–300 μm) significantly inhibited the reduction. However, to increase the kinetics, it would only need a slightly smaller particle size (if the size is below 100 μm).
3. The H<sub>2</sub> partial pressure affected the mass loss rate and the reduction mechanism. Reduction by 100% H<sub>2</sub> was 3x faster compared to 15% H<sub>2</sub>. A change of mass loss curve was identified on 100% H<sub>2</sub> reduction which may indicate a shift of reduction mechanism. The reduction mechanism at 15% H<sub>2</sub> was most likely governed by a single mechanism, implied from the gradual mass loss.

## Acknowledgments

The authors thank and acknowledge the technical support from Commonwealth Scientific and Industrial Research Organisation (CSIRO), Clayton and Spectrometer Services Pty Ltd., Melbourne, for their valuable input and the use of their facilities.

*This article is available online at AIST.org for 30 days following publication.*

## References

1. Muslemani, H.; Liang, X.; Kaesehage, K.; et al., "Opportunities and Challenges for Decarbonizing Steel Production by Creating Markets for 'Green Steel' Products," *J. Clean. Prod.*, Vol. 315, 2021, p. 128127, <https://doi.org/10.1016/j.jclepro.2021.128127>.
2. Chen, F.; Mohassab, Y.; Jiang, T.; et al., "Hydrogen Reduction Kinetics of Hematite Concentrate Particles Relevant to a Novel Flash Ironmaking Process," *Metall. Mater. Trans. B Process Metall. Mater. Process. Sci.*, Vol. 46, 2015, pp. 1133–1145, <http://dx.doi.org/10.1007/s11663-015-0332-z>.
3. Li, S.; Zhang, H.; Nie, J.; et al., "The Direct Reduction of Iron Ore With Hydrogen," *Sustain*, Vol. 13, 2021.
4. Choi, M.E., and Sohn, H.Y., "Development of Green Suspension Ironmaking Technology Based on Hydrogen Reduction of Iron Oxide Concentrate: Rate Measurements," *Ironmak. Steelmak.*, Vol. 37, 2010, pp. 81–88.
5. Sohn, H.Y.; Fan, D.Q.; and Abdelghany, A., "Design of Novel Flash Ironmaking Reactors for Greatly Reduced Energy Consumption and CO<sub>2</sub> Emissions," *Metals (Basel)*, Vol. 11, 2021, pp. 1–28.
6. Abolpour, B.; Afsahi, M.M.; and Azizkarimi, M., "Hydrogen Reduction of Magnetite Concentrate Particles," *Miner. Process. Extr. Metall. Trans. Inst. Min. Metall.*, Vol. 130, 2021, pp. 59–72, <https://doi.org/10.1080/25726641.2018.1521576>.
7. Spreitzer, D., and Schenk, J., "Reduction of Iron Oxides With Hydrogen – A Review," *Steel Res. Int.*, Vol. 90, 2019.
8. Calix Ltd., <https://calix.global/?s=zesty>.
9. Boot-Handford, M.E.; Dufty, T.; Nuraeni, B.A.; Ignacio, I.R.; Xia, Y.; Adipuri, A.; Gill, M.; Okely, A.; Hodgson, P.; Sceats, M.; and Brooks, G.A., "Calix' Zero Emissions Steel Technology (ZESTY) – Flash Hydrogen Direct Reduction of Low-Grade Ores to Green Iron and Steel Products," *METEC & 6th ESTAD*, 2023.
10. Ignácio, I.R.; Brooks, G.; Pownceby, M.I.; Rhamdhani, M.A.; Rankin, W.J.; and Webster, N.A.S., "Porosity, Mineralogy, Strength, and Reducibility of Sinter Analogues From the Fe<sub>2</sub>O<sub>3</sub> (Fe<sub>3</sub>O<sub>4</sub>)-CaO-SiO<sub>2</sub> (FCS) Ternary System," *Minerals*, Vol. 12, 2022, p. 1253, <https://doi.org/10.3390/min12101253>.
11. Nuraeni, B.A.; Avarmaa, K.L.; Prentice, L.H.; Rankin, W.J.; and Rhamdhani, M.A., "Hydrogen Reduction of LiCoO<sub>2</sub> Cathode Material: A Kinetic Study," *Metallurgical and Materials Transactions B*, Vol. 55, No. 1, 2024, pp. 319–336, <https://doi.org/10.1007/s11663-023-02960-9v>.
12. Riott, J., "Determining Metallic Iron in Iron Oxides and Slags," *Industrial & Engineering Chemistry Analytical Edition*, Vol. 13, No. 8, 1941, pp. 546–549, <https://doi.org/10.1021/i560096a011>.
13. International Organization for Standardization, "Direct Reduced Iron - Determination of Metallic Iron - Bromine-Methanol Titrimetric Method (ISO Standard No. 5416:2006), 2006, <https://www.iso.org/standard/39727.html>.
14. Farren, M.; Matthew, S.; and Hayes, P., "Reduction of Solid Wustite in H<sub>2</sub>/H<sub>2</sub>O/CO/CO<sub>2</sub> Gas Mixtures," *Metallurgical Transactions B*, Vol. 21, 1990, pp. 135–139.
15. Fruehan, R.; Li, Y.; Brabie, L.; and Kim, E.J., "Final Stage of Reduction of Iron Ores by Hydrogen," *Scandinavian Journal of Metallurgy*, Vol. 34, No. 3, 2005, pp. 205–212.
16. Kim, W-H.; Lee, S.; Kim, S-M.; and Min, D-J., "The Retardation Kinetics of Magnetite Reduction Using H<sub>2</sub> and H<sub>2</sub>-H<sub>2</sub>O Mixtures," *International Journal of Hydrogen Energy*, Vol. 38, No. 10, 2013, pp. 4194–4200, <https://doi.org/https://doi.org/10.1016/j.ijhydene.2013.01.147>.



This paper was presented at AISTech 2024 — The Iron & Steel Technology Conference and Exposition, Columbus, Ohio, USA, and published in the AISTech 2024 Conference Proceedings.

### Did You Know?

#### Cemvion Turns EAF, BOF Slags Into SCM

Cemvion announced it has developed technology which transforms electric arc furnace (EAF) and basic oxygen furnace (BOF) slags into supplementary cementitious material (SCM) while recovering valuable metals.

Of the 55 million metric tons of steel slag generated yearly in the EU, an estimated 52% is currently underutilized and often ends up in landfills or directed to other low-value applications. As EAFs and direct reduced iron (DRI) replace BOFs, granulated blast furnace slag (GBS) availability declines. EAF slag has remained underutilized due to its chemical composition and high metal and impurity content, the company said.

"Our process enables high-performing cement products from materials that would otherwise be treated as waste. With this innovation, we're proving that decarbonization and circularity can go hand in hand, and at scale," said Oscar Hållén, chief executive officer of Cemvion.

The patent-pending beneficiation process upcycles slag into SCM which is on par with, or outperforms, ground granulated blast furnace slag (GGBS), according to third-party testing. Of the 25–40% iron oxide in EAF slag, Cemvion's slag valorization process can extract and recover an estimated 99%. The iron and other valuable materials such as chromium can be returned to steel producers and reintroduced to the steelmaking process with a circular material loop.

The company said the output material helps secure feedstock of its Re-Ment Massive and Rapid and can be used as a clinker replacing SCM to ensure and extend circularity in the cement industry.

Cemvion has worked with metallurgical research institute Swerim to develop this innovation. Together, they said they have proven both technical feasibility and commercial potential.